Near Surface Geophysics, 2010, **8**, 287-296 doi:10.3997/1873-0604.2010018

Geophysical investigation for the rehabilitation of a flood control embankment[§]

E. Cardarelli, M. Cercato[*] and G. Di Filippo

'Sapienza' University of Rome, D.I.T.S. Area Geofisica, Via Eudossiana 18, 00184 Rome, Italy

Received March 2010, revision accepted May 2010

ABSTRACT

To comply with recently published seismic regulations and environmental standards, existing dams and embankments have to be evaluated for safety control, in addition to standard maintenance and repair, which is common practice for aging structures. In either case, engineering geophysics is almost the only viable option for investigating these structures and the underlying soil as a whole. In this contribution, electrical and seismic surveys are performed on an outdated flood control embankment that is expected to be put into service again. Integration of DC resistivity results with those of various seismic prospecting methods (seismic refraction, cross-hole S-wave and P-wave tomography and surface wave analysis) is found to be successful for defining a clear physical representation of the entire structure. The low-strain elastic properties (from seismic speeds of propagation) as well as the geometrical characteristics of the internal core of the dam and of the foundation soil serve as guidance for the rehabilitation intervention.

INTRODUCTION

Dam safety assessment has received considerable attention in recent years. New seismic and environmental regulations, as well as improved design capability, today set higher standards for dam safety design and analysis. To comply with these standards, existing dams and embankments are now being checked for maintenance, repair or rehabilitation. To design the rehabilitation intervention, the integrity of the embankment must be carefully evaluated, especially for aging or inactive structures where, based on present regulations, the stability of the dam under static and dynamic conditions is not theoretically verifiable, since it is not known how much the structure has deteriorated through the years. To this end, geophysical investigations are highly recommended to investigate non-invasively the structure and the subsoil. Once a quantitative physical model of the dam is built through integration of geophysical results and other types of investigation (geotechnical, mechanical, direct inspection), common intervention strategies may include: improvement of the mechanical properties of the dam material (consolidation or *in-situ* densification), modification of the dam's shape (especially for earth dams), renewal and improvement of the drainage system etc.

Since early developments (Bogoslovsky and Ogilvy 1970), the application of geophysical methods to earthen dam structures has increased (Butler *et al.* 1989, 1990) and it is nowadays considered a well-established tool for dam investigation, as confirmed by recent developments (Sjödahl *et al.* 2009; Bolève *et al.* 2009). In the previous literature on this subject, attention was mainly focused on the evaluation of the seepage phenomena that took place within earthen dams. More specifically, since unplanned seepage is the most frequent cause for embankment dam failures, the use of geophysical methods to detect and map anomalous flow pathways is considered an important safety-assessment tool (Butler *et al.* 1989, 1990). Surface and cross-well electrical DC methods (Johansson and Dahlin 1996; Cho and Yeom 2007; Sjödahl *et al.* 2009) have been extensively used to map seepage-induced resistivity changes, as well as preferential flow pathways associated with lowered resistivity values within the structure (Sjödahl *et al.* 2006, 2008). The electrokinetic phenomenon of streaming potential (Sill 1983) has been also exploited for embankment dam seepage monitoring and detection (Al-Saigh *et al.* 1994; Panthulu *et al.* 2001; Sheffer and Howie 2003; Bolève *et al.* 2009) because of the sensitiveness of self-potential measurements to groundwater flow. Since anomalous seepage often appears in association with the progressive internal erosion of the dam's impervious core, low-velocity zones within the dam's body have been investigated using radar techniques (Carlsten *et al.* 1995) and seismic reflection (Butler *et al.* 1990). An integrated approach involving different geophysical data and their joint interpretation (Butler *et al.* 1989; Kim *et al.* 2007) or merging geophysical data with geotechnical data (Oh and Sun 2008) is often a cost effective method to provide a physical model of the dam. As a matter of fact, in all the above papers the field measurements are mainly focused on

[§] This paper is based on the extended abstract A19 presented at the 15th EAGE Near Surface 2009 meeting, 7–9 September 2009, Dublin, Ireland.

[*] michele.cercato@uniroma1.it

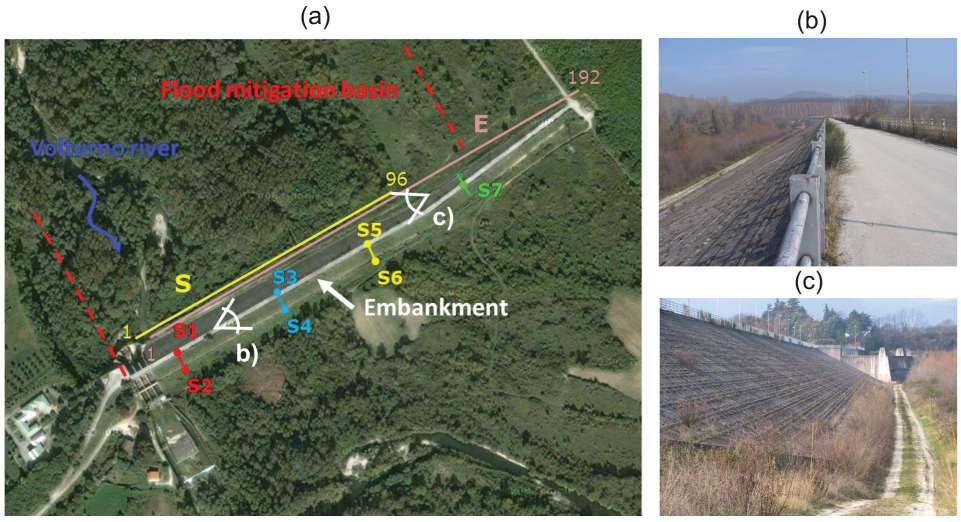

FIGURE 1
a) Location map of the survey site. The ERT roll-along line is indicated as 'E', whereas the seismic line as 'S'. The four seismic tomography cross-sections are labelled S1–S2, S3–S4, S5–S6 and S7, respectively. b–c) Views from opposite directions of the embankment.

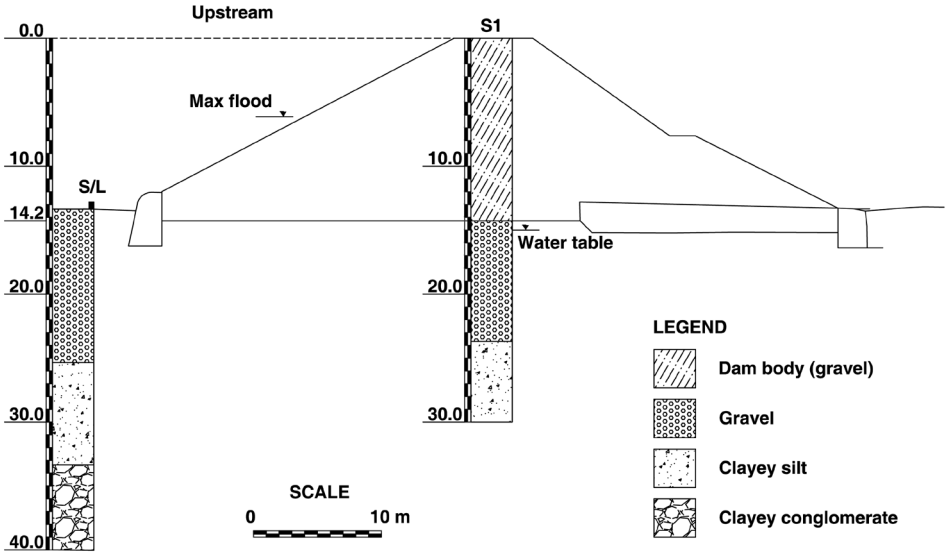

FIGURE 2
Cross-section of the embankment with the reference geological stratigraphy for the area between boreholes S1 and S5.

seepage evaluation and more specifically, on the investigation of groundwater flow within the embankment's impervious core.

Although earthen dams have been preferred as the subject of geophysical investigations for obvious logistic reasons (structure accessibility, moderate slope inclinations and seepage evaluation within the natural material filling), some applications of geophysical methods to concrete dams are also reported in the geophysical literature (Frasheri *et al.* 1999; Karastathis *et al.* 2002), where the structure is investigated by using seismic techniques for the detection of cracks and fractures.

A new problem that has recently emerged, because of newly published seismic codes (CEN 2003), is the seismic verification of existing dams and embankments, either for operating structures or for outdated structures to be put again into service. According to modern seismic codes, the design spectra for seismic analysis are site-dependent, since their computation depends, among other parameters, on the soil classification based on the Vs,30 parameter, which is a weighted average of the shear-wave velocity in the shallower 30 m below the structure (CEN 2003).

Consequently, two main issues need to be addressed regarding subsoil characterization for the seismic verification of existing structures: first, evaluation of the structure's integrity (layering and geometry of the internal core) and, second, evaluation of the shear velocity of the soil and rock underlying the embankment.

To this end, it is described how the application of integrated geophysical surveys, mainly oriented to seismic safety assessment, can be used for the characterization of an outdated rock-fill embankment, to be restored and put back into service for flood mitigation.

SITE DESCRIPTION, ACQUISITION AND INTERPRETATION METHODS OF EXPERIMENTAL DATA

The embankment under examination is a rock-fill dam with an impermeable upstream membrane; it was built in the 60s on the Volturno River in Central Italy for flood mitigation. The dam body, made of gravelly material, has a maximum height of 14.3 m and overall length of 600 m. The site map, together with

the location of the geophysical surveys are shown in Fig.1(a), whereas two views of the embankment from opposite directions are shown in Fig. 1(b,c).

After more than ten years of disuse, it is planned to put this structure into service again; therefore, it was required to investigate its structural integrity and to verify its seismic safety, in compliance with the new Italian seismic code introduced in January 2008. According to the new seismic zonation of Italy, the expected peak acceleration for this site is 0.275g (website: http://zonesismiche.mi.ingv.it).

The main tasks of the geophysical investigations are to image the internal core of the embankment, in order to verify if the structure is still compliant with the original design and to assess the geometrical features and the seismic velocities of the soil underlying the structure, with the purpose of calculating the design spectra for seismic verification. Since the structure is designed for flood mitigation, the embankment is completely above the water level under standard hydraulic conditions. Consequently, the geophysical surveys were performed under such conditions, without seepage occurring in the dam body. The water table is determined from borehole S1 (Fig. 2) to be at about 15 m of depth.

As shown by borehole data, the earthen dam lies above an almost horizontally layered stratigraphy consisting of alluvial deposits of different grain sizes (Fig. 2). The dam body and its shallow-soil foundation consist of gravelly deposits, overlying a low-permeability layer of silt (ranging from clayey to sandy along the dam axis). Below this layer, clayey conglomerates are identified by the stratigraphy of the borehole drilled upstream of the embankment. A key issue in this geological scenario is to verify the lateral homogeneity of the low-permeability silty layer, so that potential preferential drainage pathways below the dam body can be detected.

To this end, seismic prospecting was chosen to be the leading investigation method and both borehole and surface seismic sur-

TABLE 1
Acquisition parameters for borehole and surface seismic investigations

ID (Fig. 1)	Description	Acquisition parameters and instrumentation
S1–S2 S3–S4 S5–S6 S7	Borehole P-wave tomography (Fig. 3)	7 Hz vertical land-case geophones 7 Hz vertical borehole geophones Number of active channels: 24 Dt = 31 μs Ns = 16384 Source: Borehole P-wave sparker
S3–S4	Borehole S-wave tomography and S-wave borehole log	7 Hz horizontal land-case geophones Number of channels: 24 Dt = 31 μs Ns = 16384 Source: Borehole SH-wave sparker
S	Surface refraction tomography and multichannel analysis of surface waves (MASW) (Fig. 4)	7 Hz vertical land-case geophones Number of shots: 20 Number of channels: 48 40 m max source offset Dx = 2 m Dt = 0.125 ms Ns = 16384 Source: shotgun

TABLE 2
Acquisition parameters for electrical tomography investigations

ID (Fig. 1)	Description	Acquisition parameters and instrumentation
E	Electrical resistivity tomography (ERT)	Roll-along sequence 6 leapfrogging Dx = 3m Pole-dipole array Number of electrodes: 192 Number of measures: 5223 Device: Iris Syscal Pro 48

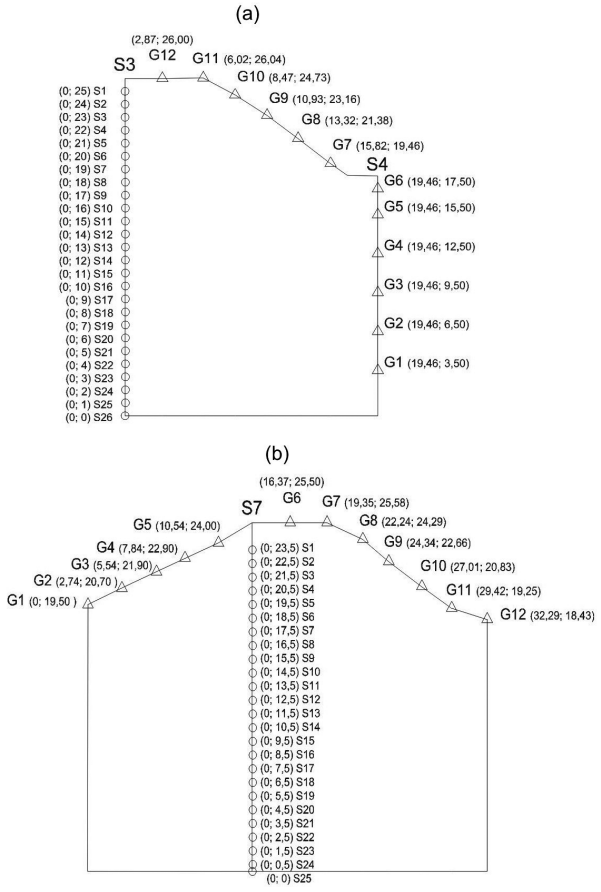

FIGURE 3

Two examples of the acquisition layout for seismic tomography cross-sections. a) S5–S6 cross-section. b) S7 cross-section. Distances are in metres.

veys were performed to image the earthen dam body and its underlying soil. In addition, electrical tomography (ERT) was performed to integrate the seismic velocity sections with independent data and to confirm certain geological features, principally the location of the water table and the continuity of the low permeability silty unit (Fig. 2). The main parameters of the geophysical surveys performed on the dam are reported in Tables 1 and 2, where the surveys are labelled according to Fig. 1.

In this case study, the P-wave velocity variations within the embankment can be associated with variations of the elastic properties of the dam rock-fill material because the embankment is totally above the water level. Consequently, four seismic P-wave tomography cross-sections were performed along the axis of the embankment to examine the seismic velocity variations within the rock-fill core. The seismic cross-sections are labelled S1–S2, S3–S4, S5–S6 and S7, respectively, after the boreholes shown in Fig. 1.

The acquisition geometry of the cross-well P-wave tomographic sections was planned according to changes in the shape of the section along the embankment's axis. Two examples of

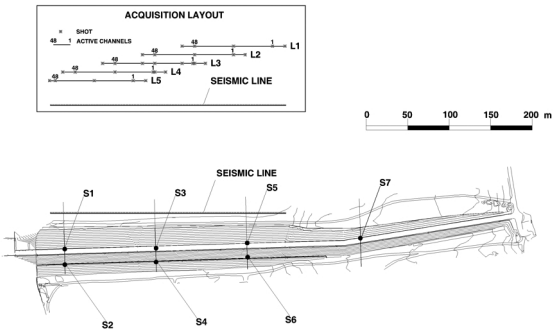

FIGURE 4

Acquisition layout for the seismic surface investigations (line S in Fig. 1a).

different acquisition geometry are displayed in Fig. 3. The cross-hole acquisition geometry presented in Fig. 3(a) is drawn for the S3–S4 cross-section but is also applicable to the S1–S2, S5–S6 cross-sections because the shape of the embankment does not change significantly between sections S1–S2 and S5–S6. In each case, the seismic source was placed in the borehole drilled on the embankment's top, six vertical land-case geophones were deployed along the downstream slope of the dam and six vertical marsh-case geophones were deployed in the shallow borehole drilled at the downstream toe of the embankment. Figure 3(b) is drawn for the S7 cross-section where the seismic source was placed in a single borehole at the top of the embankment and vertical land-case geophones were emplaced on both the upstream and the downstream slopes for a total of twelve active channels. In addition to the P-wave tomography cross-sections, an S-wave shallow tomography was performed at the S5–S6 cross-section in order to image the shear-wave velocity of the upper part of the dam, which is directly linked to the dam's shear stiffness. In the case of S-wave tomography, horizontal land-case geophones are deployed along the downstream slope of the embankment. For each source position, multiple shots are fired, reversing the source direction at least once to take advantage of the S-wave polarization when picking the shear-wave traveltimes. In each case, the seismic borehole source is a modular borehole sparker (nominal impulse energy 1 kJ) capable of maximizing the generation of either P-waves or SH-waves by the installation of different steel casings on the probe.

The P- and S-wave traveltimes are inverted by iterative (conjugate gradient) least squares (Cardarelli and de Nardis 2001), employing the ray-tracing approach of the linear traveltime interpolation method (Asakawa and Kawanaka 1993) as the forward problem solver (Cardarelli and Cerreto 2002).

An electrical resistivity tomography (ERT) line (labelled 'E' in Fig. 1) was acquired on the upstream side of the embankment, parallel to its axis, to evaluate the heterogeneity and the geometry of the soil underlying the dam as well as to verify the continuity of the silty layer. The electrical array consists of 192 electrode positions spaced 3 m apart (573 m overall length). Data were collected

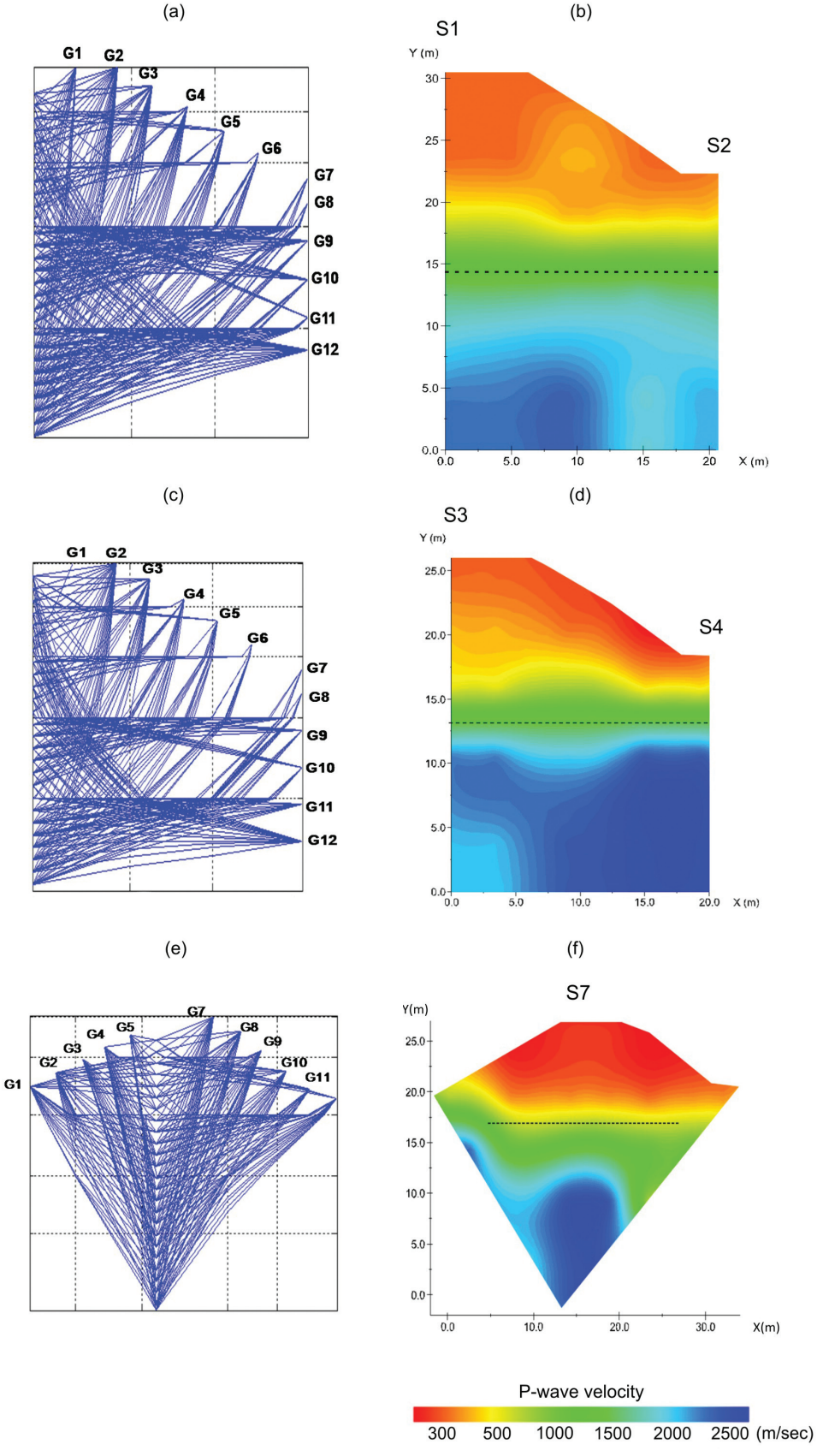

FIGURE 5
P-wave seismic tomographic cross-sections of the embankment taken at various positions along the axis of the dam. Boreholes are located in Figs 1(a) and 4. a) Ray tracing for the S1–S2 P-wave velocity section (b). c) Ray tracing for the S3–S4 P-wave velocity section (d). e) Ray tracing for the S7 P-wave velocity section (f).

with a pole-dipole acquisition scheme in a roll-along sequence. Resistivity data were inverted by Res2Dinv© (Loke and Barker 1996) using smoothness-constrained least squares inversion.

In addition, a surface seismic line (labelled 'S' in Fig. 1a) was partially superimposed on the ERT line (labelled 'E' in Fig. 1a) and acquired according to the field geometry shown in Fig. 4. In brief, using the acquisition parameters described in Table 1, seismic refraction tomography and surface wave data were collected simultaneously using a roll-along scheme that employed five linear arrays of 48,7-Hz geophones spaced 2 m apart. Symmetric shots were executed to point out possible lateral variations within the dam body. A seismic refraction tomography section is obtained by inverting the first arrival P-wave data of the central part of the seismic line. Data are inverted using the same algorithm adopted for the cross-well tomographies described above (Cardarelli and Cerreto 2002; Cardarelli *et al.* 2009).

For surface-wave processing, data were re-sampled to 2 ms and phase-shift transformed in the phase velocity-frequency (*f-c*) domain (Xia *et al.* 2007), where the experimental Rayleigh-wave dispersion is determined by picking the maxima of the transformed spectrum, which are the loci that satisfy the dispersion relation (McMechan and Yedlin 1981). This way, the experimental dispersion ensemble is computed by averaging data over the entire seismic line. Data inversion is performed by very fast simulated annealing (Cercato *et al.* 2010) obtaining the inverted 1D S-wave profiles and the associated uncertainty.

GEOPHYSICAL RESULTS

The results of the geophysical investigations will be described in the following with reference to the two main objectives described

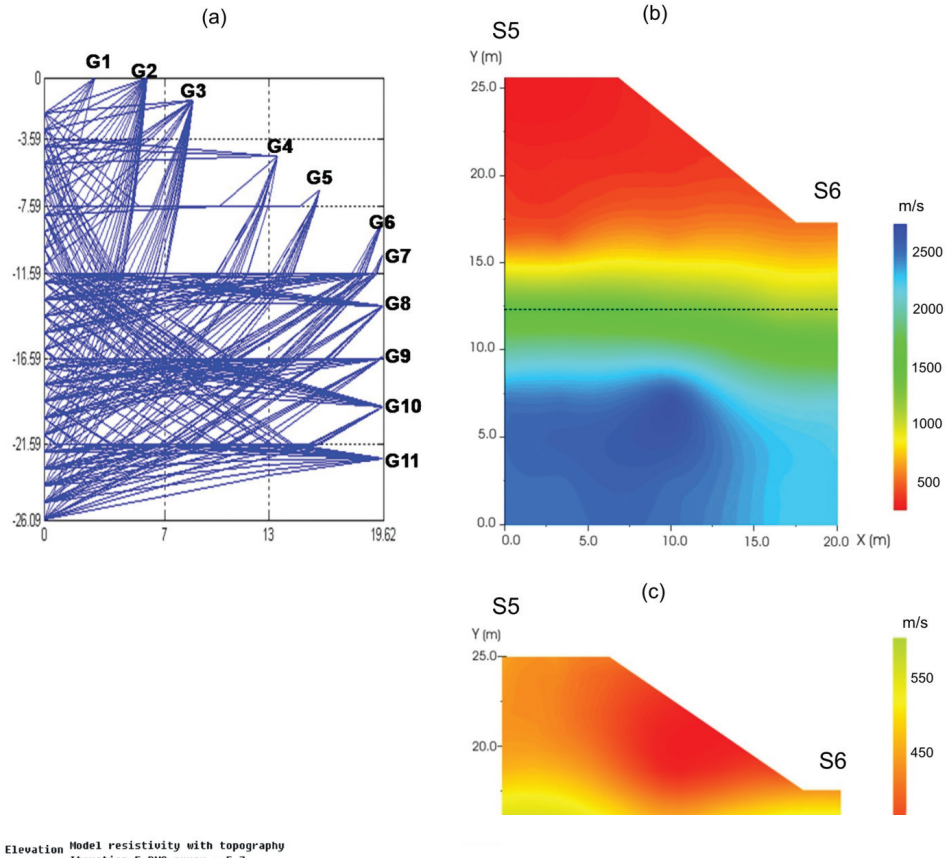

FIGURE 6
Crosswell seismic tomography S5–S6. a) Ray tracing for the P-wave velocity section (b). c) S-wave velocity cross-section.

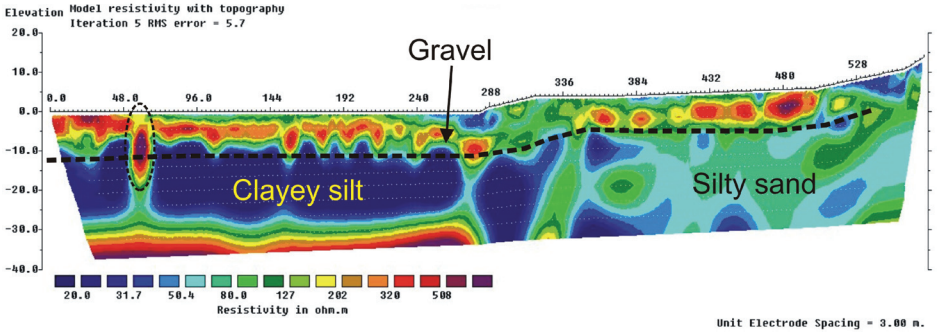

FIGURE 7
Electrical resistivity tomography. Inverted resistivity section for the E roll along the ERT line located in Fig. 1(a).

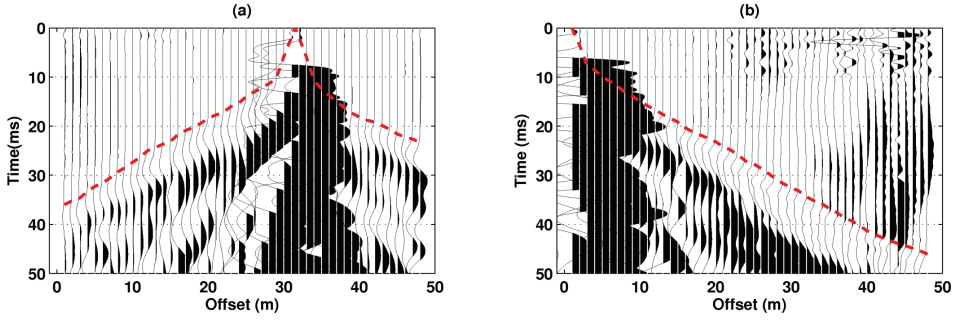

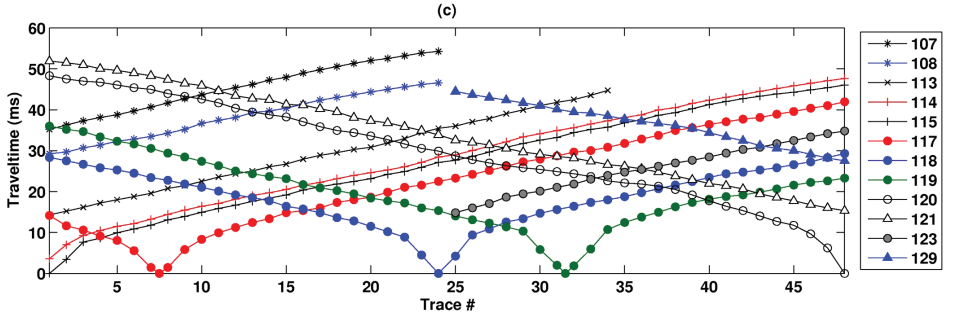

FIGURE 8
Seismic refraction tomography. a–b) Example shot gathers with picked first arrivals. c) Traveltime curves for the seismic S line located in Fig. 1(a).

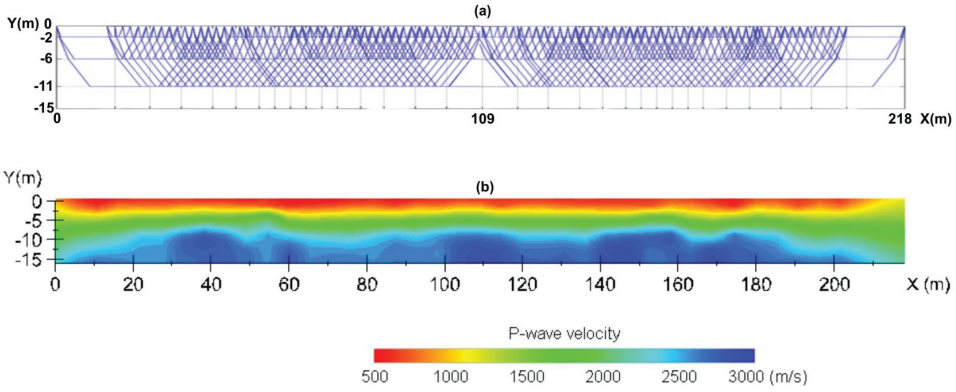

FIGURE 9
Seismic refraction tomography inversion of the traveltime curves in Fig. 8(c). a) Ray tracing of inverted model (b).

above: the investigation of the dam's internal core and the characterization of the geometry and of the elastic properties of the subsoil underlying the dam.

Characterization of the embankment's internal core

The interior of the embankment was surveyed by seismic tomography that imaged the seismic velocities of the rock-fill material.

In Fig. 5 we compare the P-wave tomographic cross-sections of the embankment taken at various positions along the embankment's axis (Fig. 1). For each section, both the inverted P-wave velocity model and the associated ray tracing are displayed. It can be noticed that the inverted tomographic sections are fairly similar along the axis of the structure, pointing out the same P-wave velocity range (400–1000 m/s) for the low-consolidated gravel in the dam. On the contrary, the gravel on which the embankment is founded, compacted by heavy tamping before construction, exhibits higher P-wave velocity values. The P-wave sections displayed in Figs 5 and 6 indicate that the elastic stiffness beneath the embankment (whose limit is marked by the dashed lines in Figs 5b, 5d, 5f and 6b) is gradually increasing and has a maximum compressional velocity of 2500 m/s. The percentage RMS errors are quite similar (around 5%) for all the tomographic inversions.

The P- and S-wave velocity tomographies of the S5–S6 cross-section are displayed in Fig. 6. The velocity distribution in this section is similar to the S1–S2 and S3–S4 tomographic sections (Figs 5b and 5d). The S-wave tomography is focused on the upper part of the dam. When compared to the P-wave tomography, the S-wave tomography involves shorter source-receiver distances and a reduced ray-coverage due to the small number of S-wave receivers available for the survey. Under these circumstances, straight raypaths can be reasonably assumed. Therefore, the S-wave tomographic inversion was performed under the straight raypaths approximation: for this reason the S-wave ray tracing is not displayed in Fig. 6.

From these results it can be concluded that the embankment's internal core exhibits elastic properties that do not vary substan-

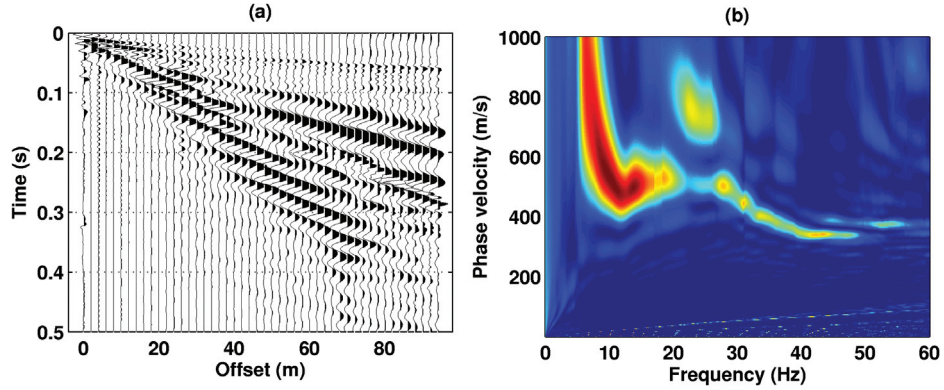

FIGURE 10
MASW survey. a) Example shot gather. b) Phase velocity – frequency spectrum of the shot gather (a).

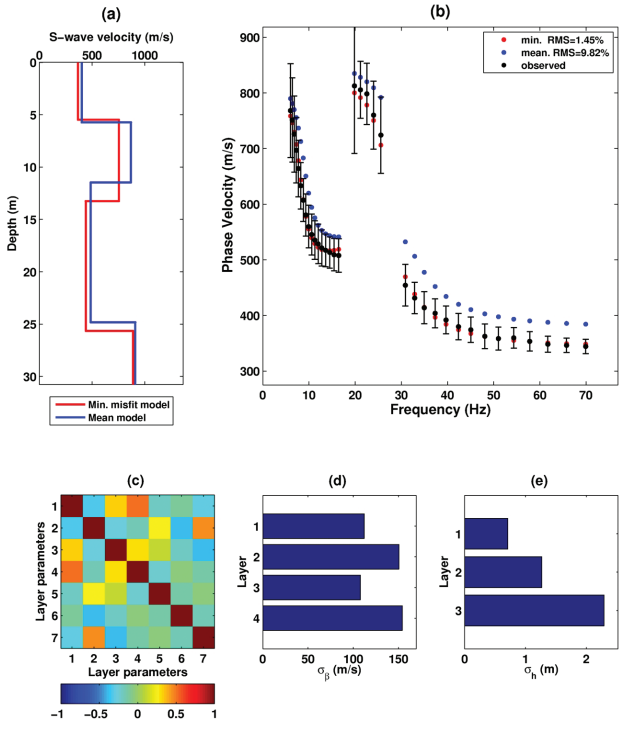

FIGURE 11
MASW very fast simulated annealing inversion. a) Mean model (blue solid line) and minimum misfit model (red solid line) obtained by modal VFSA inversion. b) Observed and predicted dispersion curves. c) Posterior correlation matrix. The first four layer parameters correspond to layer shear-wave velocities whereas the last three (5–7) correspond to layer thicknesses. d) Uncertainty estimation for layer shear velocities. e) Uncertainty estimation for layer thicknesses.

tially along the embankment's axis. When compared to the borehole stratigraphy, the seismic velocity values are consistent with the geological units and are increasing monotonically with depth.

Soil foundation characterization

Surface seismic and electrical surveys were performed at the upstream toe of the embankment (Fig. 1). The results obtained by the electrical resistivity tomography (ERT) inversion of the roll-along line E (Fig. 1a) are shown in Fig. 7. The inverted resistivity inverted model (fifth iteration, RMSE = 5.7%) may be divided into two different zones. A first area, located between 0–280 m along the horizontal axis, is characterized by regular layering and relatively flat interfaces. The shallow layer, which consists of gravel (see, for instance, the stratigraphy displayed in Fig. 2), exhibits resistivity values in the range between 300–400 Ωm, indicating a very shallow water table, consistent with the water table position retrieved from borehole S1. The vertically elongated resistive body located below the 60 m tick of the *x*-axis corresponds to a concrete intake structure and it is not a natural subsoil feature. In agreement with borehole stratigraphy, the embankment is founded on gravel (9–12 m thick), overlying a conductive layer (associated with clayey silt). Beneath this layer, another resistive structure is imaged that can be associated with the clayey conglomerates reported in the upstream stratigraphy (Fig. 2). On the other hand, the right-hand portion of the resistivity section exhibits different subsoil features, since the embankment is gradually adapted to the slope of a natural alluvial terrace, consisting of coarser alluvial deposits (mainly silty sand) below the gravelly surface layer, as confirmed by borehole S7. The resistivity values shown on the right-hand portion of the resistivity section are fairly compatible with these materials.

In Fig. 8, two example shot gathers and the traveltime curves of the L3 array (Fig. 4) are shown to illustrate the quality of the first arrival picking. The inversion results of the seismic refraction tomography (S line in Fig. 1) are displayed in Fig. 9.

From the seismic section, it can be observed that the P-wave velocity increases from the 500 m/s of the weathered surface layer to about 2500 m/s at 10–11 m of depth, with no further recognizable increase down to the lower boundary of the discretized model used for the tomographic inversion, at about 15 m depth (Fig. 9a). The seismic velocity distribution is fairly regular and the resulting earth model is a nearly flat-layered stratigraphy down to the maximum depth of investigation.

The seismic velocity distribution with depth is in agreement with the resistivity values obtained from ERT (Fig. 6), although it should be considered that the ERT section is much deeper and longer than the seismic line (Fig. 1a).

The weathered layer (500 m/s) is found to be approximately

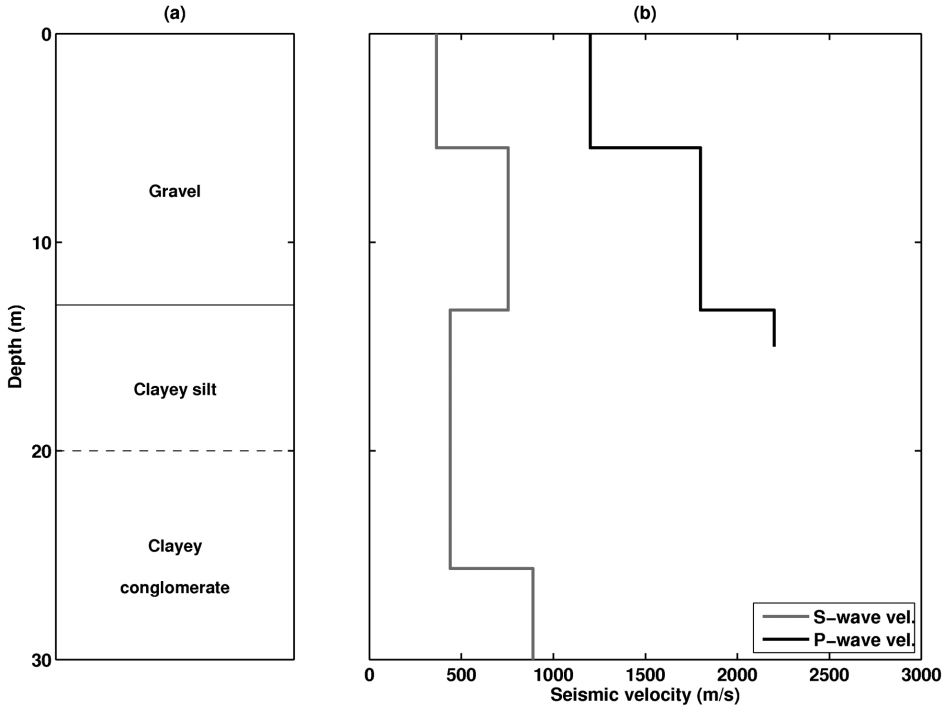

FIGURE 12
Comparison between the stratigraphic column (a) and the seismic velocity profiles (b). The S-wave profile (grey line in Fig. 12.b) is obtained through MASW inversion, while the P-wave profile is obtained by extrapolating a reference profile from the seismic tomography section in Fig. 9.

2.5–3.0 m thick along the seismic line. This depth range is consistent with that of the water table (Fig. 2).

Below the weathered layer (500 m/s), the gravelly deposits exhibit P-wave velocity values of about 1500–2000 m/s, while in the electrical section of Fig. 7 they are marked by resistivity values of about 300–400 Ωm. The deeper refractor (2500 m/s) is identified at 10–12 m of depth and it is associated with the clayey silt unit exhibiting resistivity values of 20 Ωm. The percentage RMS of the inverted section is 4%.

With regard to surface-wave interpretation, an example shot gather and the corresponding *f-c* spectrum is shown in Fig. 10. The more characteristic feature of this dataset is a mode jump to the first higher mode in the 20–30 Hz range (Fig. 10b).

The experimental dispersion ensemble obtained by averaging the picked dispersion values of the 20 shot gathers (Fig. 11b, black circles), is then inverted by VFSA (Cercato *et al.* 2010) returning the minimum misfit and mean profiles depicted in Fig. 11(a).

The minimum misfit model is the shear-wave velocity profile associated with the global minimum of the misfit function, while the mean model is computed as the mean of all the accepted models in VFSA inversion (Cercato *et al.* 2010). The posterior correlation matrix, which is a measure of the linear dependence between the parameters (Bhattacharya *et al.* 2003), is displayed in Fig. 11(c) as well as the uncertainty estimation of the inverted parameters (shear-wave velocities and layer thicknesses) in Fig. 11(d,e).

A velocity reversal is detected at about 12 m of depth. Even with the 15–20% uncertainties in the inverted shear-wave velocity (Fig.11d) this low-velocity layer is a permanent feature of the inverted profiles. When compared to the stratigraphy, it can be associated with the geologic transition between gravelly deposits and silty (from clayey to sandy silt) formations, well in agreement with the ERT results of Fig. 7 and borehole data.

In Fig. 12 the stratigraphic column (Fig. 12a) of the embankment's upstream toe at the S5–S6 cross-section is compared to the seismic velocity profiles (Fig. 12b) retrieved by inversion. It can be noticed that MASW results reach greater depths when compared to seismic refraction tomography inversion (Fig. 9). More interestingly, when compared to the overlying gravel (which shows a Poisson's ratio in the range 0.37–0.39), the clayey silt deposits exhibit a reduced shear-wave velocity (450 m/s), which is responsible for an increase in the Poisson's ratio up to about 0.47. Interestingly, the reversal of S-wave velocity in the clayey silt is associated with an increase in P-wave velocity (detected by both borehole and surface tomography): this phenomenon can be explained because the water table is very shallow (Fig. 2) and plays a major role as far as P-wave velocity is concerned. Additionally, MASW inversion detects a shear velocity increase at about 25 m of depth below the ground level at the upstream embankment's toe, which is related to the presence of the clayey conglomerates (Fig. 2).

CONCLUSIONS

Although direct inspection is always necessary for seismic design, a comprehensive geophysical investigation is capable of correlating the results of borehole and geotechnical investigations, in order to build a consistent picture of the earthen dam structure and the underlying subsoil as a single system.

In the particular case study reported here, the borehole seismic investigation (S- and P-wave tomography cross-sections) assessed the elastic stiffness of the earth body, pointing out the

homogeneity of the rock-fill along the axis of the earth dam. The integration of borehole results with the resistivity section in Fig. 7 excluded the presence of anomalous foundation features, while the elastic low-strain properties of the embankment's foundation soil were determined by integration of surface wave survey and P-wave refraction tomography results. Surface-wave inversion was capable of describing a shear velocity decrease across the interface between gravel and clayey silt.

It has been demonstrated how, in the case of existing dams and embankments, geophysical prospecting is capable of investigating large volumes of the structure non-invasively and at reasonable costs, giving original information about the dam internal material. In addition, by determining the shear-wave velocity of the soil below the structure, it was possible to unequivocally obtain the seismic soil classification at the embankment's site, which is needed to determine the design spectrum required for the response analysis and the safety assessment of the structure under dynamic excitation.

Therefore, geophysical investigation should always be considered when planning the examination of existing dams and embankments, in order to build a consistent picture of the soil-structure system. On the basis of the geophysical results, the location of geotechnical and direct investigations can be optimized, reducing the number of boreholes, excavations and other invasive investigations with significant time and cost savings.

ACKNOWLEDGEMENTS

'Studio Olivero', Via Imperia 2, 00161 Rome, Italy and the 'Consorzio di Bonifica della Piana di Venafro', Via Giulia Colonia 2, 86079 Venafro (IS), Italy are thanked for their permission to publish these results. The authors are grateful to Giorgio De Donno, Francesco Pugliese and Mirko Avellini of 'Sapienza' University of Rome for their contribution to data acquisition.

REFERENCES

Al-Saigh N.H., Mohammed Z.S. and Dahham M.S. 1994. Detection of water leakage from dams by self-potential method. *Engineering Geology* **37**, 115–121.

Asakawa E. and Kawanaka T. 1993. Seismic ray tracing using linear travel time interpolation. *Geophysical Prospecting* **41**, 99–111.

Bhattacharya B.B., Shalivahan and Sen M.K. 2003. Use of VFSA for resolution, sensitivity and uncertainty analysis in 1D DC resistivity and IP inversion. *Geophysical Prospecting* **51**, 393–408.

Bogoslovsky V.A. and Ogilvy A.A. 1970. Application of geophysical methods for studying the technical status of earth dams. *Geophysical Prospecting* **18**, 758–773.

Bolève A., Revil A., Janod F., Mattiuzzo J.L. and Fry J.-J. 2009. Preferential fluid flow pathways in embankment dams imaged by self-potential tomography. *Near Surface Geophysics* **7**, 447–462.

Butler D.K., Llopis J.L. and Deaver C.M. 1989. Comprehensive geophysical investigation of an existing dam foundation, part 1. *The Leading Edge* **8**, 10–18.

Butler D.K., Llopis J.L., Dobecki T.L., Wilt M.J., Corwin R.F. and Olhoeft G. 1990. Comprehensive geophysical investigation of an existing dam foundation. Part 2: Engineering geophysics research and development. *The Leading Edge* **9**, 44–53.

Cardarelli E., Cercato M., Cerreto A. and Di Filippo G. 2009. Electrical resistivity and seismic refraction tomography to detect buried cavities. *Geophysical Prospecting* **58**, 685–695. doi:10.1111/j.1365-2478.2009.00854.x

Cardarelli E. and Cerreto A. 2002. Ray tracing in elliptical anisotropic media using linear traveltime seismic interpolation (LTI) method applied to traveltime seismic tomography. *Geophysical Prospecting* **50**, 55–72.

Cardarelli E. and de Nardis R. 2001. Seismic Refraction, isotropic and anisotropic seismic tomography on an ancient monument. *Geophysical Prospecting* **49**, 228–240.

Carlsten S., Johansson S. and Wörman A. 1995. Radar techniques for indicating internal erosion in embankment dams. *Journal of Applied Geophysics* **33**,143–156.

CEN 2003. EuroCode 8: Design of Structures for Earthquake resistance. Part 1: General Rules, Seismic Actions and Rules for Buildings. Draft 6. European Committee for Standardization, Brussels.

Cercato M., Cara F., Cardarelli E., Di Filippo G., Di Giulio G. and Milana G. 2010. Shear-wave velocity profiling at sites with high stiffness contrasts: A comparison between invasive and non-invasive methods. *Near Surface Geophysics* **8**, 75–94.

Cho I.K. and Yeom J.Y. 2007. Crossline resistivity tomography for the delineation of anomalous seepage pathways in an embankment dam. *Geophysics* **72**, G31–G38.

Frasheri A., Nishani P., Kapplani L., Xinxo E., Çanga B. and Dhima F. 1999. Seismic and geoelectric tomography surveys of dams in Albania. *The Leading Edge* **18**, 1384–1388.

Johansson S. and Dahlin T. 1996. Seepage monitoring in an earth embankment dam by repeated resistivity measurements. *European Journal of Engineering and Environmental Geophysics* **1**, 229–247.

Karastathis V.K., Karmis P.N., Drakatos G. and Stavrakakis G. 2002. Geophysical methods contributing to the testing of concrete dams. Application at the Marathon Dam. *Journal of Applied Geophysics* **50**, 247–260.

Kim J.-H., Yi M.-J., Song Y., Seol S.J. and Kim K.-S. 2007. Application of geophysical methods to the safety analysis of an earth dam. *Journal of Environmental and Engineering Geophysics* **12**, 221–235.

Loke M.H. and Barker R.D. 1996. Rapid least-squares inversion of apparent resistivity pseudosections by a quasi-Newton method. *Geophysical Prospecting* **44**, 131–152.

McMechan G.A and Yedlin M.J. 1981. Analysis of dispersive waves by wave field transformation. *Geophysics* **46**, 869–874.

Oh S. and Sun C.G. 2008. Combined analysis of electrical resistivity and geotechnical SPT blow counts for the safety assessment of fill dam. *Environmental Geology* **54**, 31–42.

Panthulu T.V., Krishnaiah C. and Shirke J.M. 2001. Detection of seepage paths in earth dams using self-potential and electrical resistivity methods. *Engineering Geology* **59**, 281–295.

Sheffer M.R. and Howie J.A. 2003. A numerical modelling procedure for the study of the streaming potential phenomenon in embankment dams. Symposium on the Application of Geophysics to Engineering and Environmental Problems, San Antonio, Texas, USA, 475–487.

Sill W.R. 1983. Self-potential modelling from primary flow. *Geophysics* **48**, 76–86.

Sjödahl P., Dahlin T. and Johansson S. 2008. Resistivity monitoring for leakage and internal erosion detection at Hällby embankment dam. *Journal of Applied Geophysics* **65**, 155–164.

Sjödahl P., Dahlin T. and Johansson S. 2009. Embankment dam seepage evaluation from resistivity monitoring data. *Near Surface Geophysics* **7**, 463–474.

Sjödahl P., Dahlin T. and Zhou B. 2006. 2.5D resistivity modeling of embankment dams to assess influence from geometry and material properties. *Geophysics* **71**, G107–G114.

Xia J., Xu Y. and Miller R.D. 2007. Generating an image of dispersive energy by frequency decomposition and slant stacking. *Pure and Applied Geophysics* **164**, 941–956.